Environment Canada

Water Science and Technology Directorate

Direction générale des sciences et de la technologie, eau

Environnement Canada

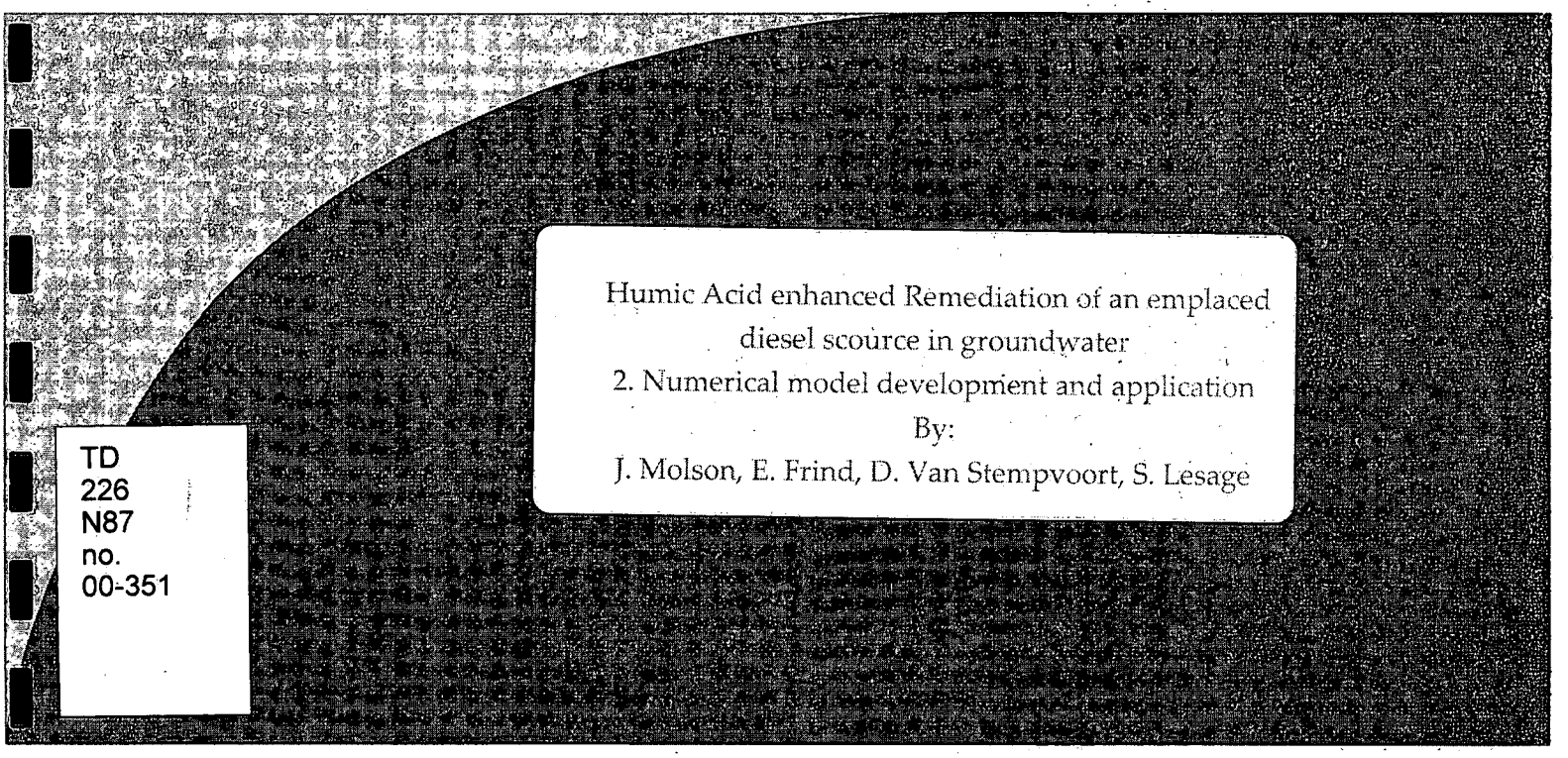

Humic Acid enhanced Remediation of an emplaced diesel source in groundwater
2. Numerical model development and application

By:
J. Molson, E. Frind, D. Van Stempvoort, S. Lesage

0-351

Molson, J.W., Frind, E.O., D. R. Van Stempvoort, D.R. and Lesage, S. Humic Acid Enhanced Remediation of an Emplaced Diesel Source in Groundwater: 2. Numerical Model Development and Application.

Management Perspective

This manuscript, prepared for publication in Journal of Contaminant Hydrology, describes research that was funded by the Centre for Research in Earth & Space Technology (CRESTech). This work is of interest to the groundwater remediation service industry in Canada. The work contributes toward Environment Canada's Clean Environment theme, with the intended result that environmental and human health threats posed by toxic substances and other substances of concern are prevented or reduced.

The manuscript reports the development of a numerical model to simulate groundwater remediation using a new technology, in situ flushing. The model was applied to a pilot scale experiment of in situ flushing of PAH contaminants from an emplaced diesel source in groundwater, using a commercial humic product as a flushing agent. This experiment was conducted at the AQUEREF facility, Canada Centre for Inland Waters, Burlington, Ontario. Processes that were modeled include: humic-assisted transport of diesel contaminants, sorption and biodegradation. Some simulations were used to demonstrate how changes in the concentration of the humic acid would affect the efficiency of groundwater remediation. A joint paper (Part 1), provides details on the pilot scale test, which was conducted by Environment Canada (NWRI).

Assainissement amélioré par l'acide humique d'une source ponctuelle de carburant diesel contaminant l'eau souterraine : 2. Développement et application d'un modèle numérique.

Molson, J. W., Frind, E. O., Van Stempvoort, D. R. et Lesage, S.

Sommaire à l'intention de la direction

Ce manuscrit, préparé pour publication dans le Journal of Contaminant Hydrology, décrit des recherches financées par le Centre for Research in Earth and Space Technology (CRESTech). Cette étude, qui est utile pour l'industrie des services d'assainissement des eaux souterraines du Canada, s'insère dans le secteur d'activité Un environnement sain d'Environnement Canada. Les résultats attendus sont la prévention ou la réduction des dangers pour l'environnement et la santé humaine posés par les substances toxiques et d'autres substances préoccupantes.

Ce manuscrit décrit le développement d'un modèle numérique destiné à simuler l'assainissement des eaux souterraines à l'aide d'une nouvelle technologie, la purge *in situ*. On a appliqué ce modèle à une expérience pilote de purge *in situ* des contaminants HAP d'une source de carburant diesel ponctuelle se diffusant dans les eaux souterraines, qui utilisait un produit commercial à base d'acide humique comme agent de purge. On a effectué cette expérience à l'installation AQUEREF du Centre canadien des eaux intérieures de Burlington (Ontario). Les processus modélisés étaient notamment le transport assisté par l'acide humique des contaminants du carburant diesel, ainsi que leur sorption et leur biodégradation. On a utilisé certaines simulations pour démontrer comment des changements dans la concentration de l'acide humique peuvent influer sur l'efficacité de l'assainissement des eaux souterraines. Un document connexe (partie 1) décrit les essais à l'échelle pilote effectués par Environnement Canada (INRE).

Abstract

A pilot scale experiment involving humic acid-enhanced diesel fuel dissolution (Van Stempvoort et al., this issue) is numerically simulated in three dimensions. The simulation approach considers the nonlinear coupled processes of multicomponent enhanced NAPL dissolution, reactive mass transport of the dissolved organics and humic acid carrier as well as aerobic biodegradation, all of which are represented in the model BIONAPL/3D. The model is calibrated with respect to dissolution and biodegradation by comparing observed and simulated concentrations of seven diesel fuel components (BTEX and methyl-, dimethyl- and trimethylnapthalene) over a 1500-day monitoring period. Independant lab data were used to obtain partition coefficients and to describe the kinetic nonlinear sorption behaviour to the aquifer solids. The observed asymmetric breakthrough of the humic acid was reproduced assuming a kinetically-limited Langmuir sorption model. The model showed an excellent fit to the observed data, and accurately reproduced the humic acid-induced 10-fold increase in apparent solubility of trimethylnaphthalene. Solubility increases on the order of 2-5 were simulated for methylnaphthalene and dimethylnaphthalene, respectively. A sensitivity analysis showed that the time required for complete source depletion was mostly dependent on the organic/humic acid partitioning coefficients, on the humic acid concentration and on the rate of NAPL dissolution. The simulations suggest that biodegradation was most active for BTEX and the remaining, unmonitored fraction of diesel fuel (including the n-alkanes), and that dissolution of the diesel source was occurring at near-equilibrium throughout the experiment. Under the experimental conditions, the residual 500 mL diesel source was almost completely dissolved and degraded within 5 years. Without humic acid flushing, complete remediation to drinking water limits would take about 5 times longer.

Résumé

On a simulé numériquement dans les trois dimensions une expérience à l'échelle pilote portant sur la dissolution du carburant diesel améliorée par l'acide humique (Van Stempvoort *et al.*; voir l'article dans ce numéro). L'approche de la simulation tient compte des processus couplés non linéaires de la dissolution améliorée des liquides non aqueux à composants multiples, du transport massique réactif des composés organiques dissous, de véhicules comme l'acide humique et de la biodégradation aérobie, qui sont tous représentés dans le modèle BIONAPL/3D. Ce modèle est étalonné pour la dissolution et la biodégradation par des comparaisons entre les concentrations observées et simulées de sept composants du carburant diesel (les BTEX et les méthyl-, diméthyl- et triméthylnapthalène), effectuées pendant une période de surveillance de 1 500 jours. On utilisait des données de laboratoire indépendantes pour obtenir des coefficients de séparation et pour décrire le comportement de sorption cynétique non linéaire par rapport aux matières solides de l'aquifère. On reproduisait la percée asymétrique observée pour l'acide humique en se basant sur l'hypothèse d'un modèle de sorption de Langmuir cynétiquement limité. Ce modèle permettait d'obtenir une excellente concordance avec les données observées, et il reproduisant avec précision l'augmentation d'un facteur 10 induite par l'acide humique pour la solubilité apparente du triméthylnaphtalène. On a simulé des augmentations de solubilité d'ordre 2 et 5 pour le méthylnaphtalène et le diméthylnaphtalène, respectivement. Une analyse de sensibilité a montré que le temps requis pour obtenir un épuisement complet de la source dépendait fortement du coefficient de séparation matières organiques/acide humique, de la concentration de l'acide humique et de la vitesse de dissolution des liquides non aqueux. Cette simulation semble indiquer que la biodégradation était plus active pour les BTEX et pour le reste de la fraction de carburant diesel non surveillée (notamment les *n*-alcanes), et que la dissolution de la source de carburant diesel survenait à des conditions proches de l'équilibre pendant toute l'expérience. Dans des conditions expérimentales, la source de carburant diesel résiduel de 500 mL était presque complètement dissoute et dégradée en 5 ans. Sans purge d'acide humique, un assainissement complet, conforme aux limites visant l'eau potable, devrait prendre environ cinq fois plus de temps.

Reprinted from

JOURNAL OF

Contaminant Hydrology

Journal of Contaminant Hydrology 54 (2002) 277–305

Humic acid enhanced remediation of an emplaced diesel source in groundwater. 2. Numerical model development and application

J.W. Molson [a,*], E.O. Frind [a], D.R. Van Stempvoort [b,1], S. Lesage [b,1]

[a] *Department of Earth Sciences, University of Waterloo, Waterloo, ON, Canada N2L 3G1*
[b] *National Water Research Institute, P.O. Box 5050, Burlington, ON, Canada L7R 4A6*

ELSEVIER

Journal
of

Contaminant Hydrology

Scope of the journal

The primary purpose of this international journal is to publish scientific articles pertaining to the contamination of groundwater. Emphasis is placed on investigations of the physical, chemical and biological processes that influence the behaviour of organic and inorganic contaminants in both the unsaturated (vadose) and the saturated zones. Articles on contamination of surface water are not included in this journal unless they specifically deal with the linkage between surface water and groundwater. This journal will strive to provide a common forum for publication of articles from a diverse group of scientists involved in investigations of groundwater contamination.

The paper used in this publication on meets the requirements of ANSI/NISO Z39.48-1992 (Permanence of Paper).

PRINTED IN THE NETHERLANDS

ELSEVIER

Journal of Contaminant Hydrology 54 (2002) 277–305

JOURNAL OF
Contaminant
Hydrology

www.elsevier.com/locate/jconhyd

Humic acid enhanced remediation of an emplaced diesel source in groundwater. 2. Numerical model development and application

J.W. Molson [a,*], E.O. Frind [a], D.R. Van Stempvoort [b,1], S. Lesage [b,1]

[a] *Department of Earth Sciences, University of Waterloo, Waterloo, ON, Canada N2L 3G1*
[b] *National Water Research Institute, P.O. Box 5050, Burlington, ON, Canada L7R 4A6*

Received 8 January 2001; received in revised form 20 July 2001; accepted 5 September 2001

Abstract

A pilot scale experiment for humic acid-enhanced remediation of diesel fuel, described in Part 1 of this series, is numerically simulated in three dimensions. Groundwater flow, enhanced solubilization of the diesel source, and reactive transport of the dissolved contaminants and humic acid carrier are solved with a finite element Galerkin approach. The model (BIONAPL) is calibrated by comparing observed and simulated concentrations of seven diesel fuel components (BTEX and methyl-, dimethyl- and trimethylnaphthalene) over a 1500-day monitoring period. Data from supporting bench scale tests were used to estimate contaminant-carrier binding coefficients and to simulate two-site sorption of the carrier to the aquifer sand. The model accurately reproduced the humic acid-induced 10-fold increase in apparent solubility of trimethylnaphthalene. Solubility increases on the order of 2–5 were simulated for methylnaphthalene and dimethylnaphthalene, respectively. Under the experimental and simulated conditions, the residual 500-ml diesel source was almost completely dissolved and degraded within 5 years. Without humic acid flushing, the simulations show complete source dissolution would take about six times longer.

Keywords: Groundwater remediation; Modeling; Humic acid; Dissolution; Solubilization; Biodegradation

1. Introduction

Under natural conditions, multi-component nonaqueous phase liquids (NAPLs) trapped within an aquifer typically dissolve very slowly, taking several decades or longer to

* Corresponding author. Fax: +1-519-746-7484.
E-mail address: molson@uwaterloo.ca (J.W. Molson).
[1] Fax: +1-905-336-6430.

0169-7722/02/$ - see front matter
PII: S0169-7722(01)00181-4

completely dissolve. Conventional pump-and-treat technology is often not a practical option under these conditions. Much of the current NAPL remediation research is therefore focussing on enhanced dissolution processes in which the effective source dissolution rate is increased by introducing a flushing agent to which aqueous hydrophobic organic contaminants (HOCs) can partition. Possible approaches, for example, include flushing a residual NAPL source with surfactants, cosolvents or dissolved natural organic matter (NOM).

Surfactants have shown excellent promise as an NAPL remediation option due to their high solubilization potential (Danzer and Grathwohl, 1998; Brusseau et al., 1999). Some surfactants, however, can be toxic to the indigenous microbes (Lewis, 1991; Rouse et al., 1994), they can act as preferred carbon sources over organic contaminants (Tiehm, 1994), and can reduce contaminant bioavailability (Guha and Jaffe, 1996; Zhang et al., 1997). Surfactants and cosolvents also tend to reduce the NAPL–water interfacial tension (IFT) to a greater degree than NOM (Johnson and John, 1999). While this is often used to advantage (Martel et al., 1998; Grubb and Sitar, 1999), reducing the IFT may be undesirable if, for example, there is a risk of downward mobilization to an underlying aquifer. At contaminated sites requiring NAPL solubilization but not mobilization, surfactants and cosolvents may not be the best choice.

Natural organic matter is now receiving increased attention as an alternative to surfactants and cosolvents for NAPL remediation. NOM is a relatively inexpensive, naturally occurring product of organic matter decay, it is non-toxic to microbes and binds well with HOCs (McCarthy and Jiminez, 1985; Chiou et al., 1986; Johnson and John, 1999). In contrast to surfactants, humic acid concentrations do not have to reach a critical micelle concentration for enhanced solubilization (Lesage et al., 1997; Guetzloff and Rice, 1994). In a comparison of enhanced TCE solubility using six flushing agents, including surfactants, complexing agents and alcohol, Boving and Brusseau (2000) found humic acid to be most efficient on a molar basis, and found no residual mobilization. NOM is also of interest for its ability to mobilize metals (Bryan et al., 1997) and radionuclides (McCarthy et al., 1998; Warwick et al., 2000).

A significant fraction of NOM is often composed of dissolved humic substances (DHS), including humic acid (HA), a mixture of complex macromolecular compounds to which dissolved organic contaminants are readily bound (McCarthy and Zachara, 1989). Humic substances have been studied in great detail over the past decade, primarily with respect to their potential use as a carrier for contaminant remediation (Abdul et al., 1990; Magee et al., 1991; Johnson and John, 1999).

2. Insight from existing numerical models

The processes which are fundamental to the current simulation problem include groundwater flow, dissolution of a residual NAPL, advective–dispersive transport, biodegradation, sorption of aqueous contaminants to a mobile carrier, and sorption of free and carrier-bound contaminants to aquifer solids. The NAPL may have multiple components and the dissolution, sorption and biodegradation processes may be rate-limited. Ideally, the processes should be considered within a fully 3D dynamic system.

Several models have been developed in the past which address some, but not all of these processes together. Simulation models for NOM-facilitated transport have been developed, for example, by Corapcioglu and Jiang (1993), Liu and Amy (1993), Johnson et al. (1995), Knabner et al. (1996), Rebhun et al. (1996), Totsche et al. (1997) and Johnson (2000). A review of some earlier models for NOM transport in aquifer columns is provided by Jardine et al. (1992).

Various conceptual models and numerical solution approaches have been used and most models can be applied to a variety of carriers. Ibaraki and Sudicky (1995), for example, presented a 2D finite element model for single-contaminant, colloid-facilitated transport in discretely fractured porous media. Their approach included a two-site sorption model and first-order decay of the contaminant. McCarthy et al. (1996) applied a 3D numerical model to simulate a field injection test of natural organic matter in an uncontaminated sand aquifer. Deviations between some observed and simulated NOM-breakthrough curves were thought to result from the complex mixture of different NOM subcomponents. Sorption of the NOM to the aquifer solids was derived indirectly by comparing travel times with those from a simulated conservative tracer.

A versatile simulation approach which is applicable to a variety of surfactants, cosolvents and natural organic matter was presented by Ji and Brusseau (1998). They developed a model that simulates transport of the free aqueous phase contaminant and carrier-sorbed pseudo-phase as a single component, which saves computational effort. Their model included kinetic NAPL dissolution and two-rate (equilibrium/kinetic) sorption of the carrier to the aquifer solids; however, biodegradation was not considered. The model was tested against two 1D experiments assuming a Freundlich isotherm for the flushing agents.

Additional models incorporating various combinations of enhanced NAPL dissolution, contaminant degradation and sorption have been presented by Corapcioglu and Kim (1995), Guha and Jaffe (1996), Grimberg et al. (1996), Zhang et al. (1997) and Ramaswami and Luthy (1997); however, all are limited to various degrees in the number of processes or components included. Grimberg et al. (1996) and Zhang et al. (1997), for example, develop models for simulating surfactant-enhanced dissolution, and biodegradation, but only consider a single component (phenanthrene) in simplified batch systems. Hunter et al. (1998) present a comprehensive model for simulating multi-component transport and microbially driven redox processes in groundwater but do not include NAPL dissolution or carrier transport. Most recently, Mayer et al. (submitted for publication) have developed one of the most advanced multi-component reactive transport models to date, including unsaturated flow and kinetic geochemical reactions.

Despite the recent advances in numerical models for simulating carrier-enhanced NAPL remediation, fully three-dimensional (3D) simulation approaches remain scarce. Furthermore, kinetic electron acceptor-limited biodegradation of aqueous contaminants has not yet been simulated in a multi-component, NOM enhanced NAPL dissolution problem, even though one of the primary functions of using NOM for NAPL remediation is to promote natural attenuation. Indeed, there appears as yet no existing model for simulating such a system.

In this paper, a comprehensive numerical model (BIONAPL) is developed to simulate the coupled processes of kinetic multi-component carrier-enhanced NAPL dissolution,

solubilization, biodegradation and advective–dispersive transport within a saturated system. Sorption of the humic acid carrier to aquifer solids is included as a mixed, two-site equilibrium/kinetic process. The model is tested against an analytical solution for transport with two-site sorption to solids, and is applied to simulate the humic acid-enhanced diesel remediation experiment described in Part 1 (Van Stempvoort et al., this issue).

3. Theoretical development

3.1. The conceptual model

The conceptual model is based on a residual (immobile) NAPL source dissolving into a saturated groundwater zone (Fig. 1). Whereas a residual DNAPL may be present throughout the saturated and unsaturated zones, a residual LNAPL such as diesel fuel will pool at the watertable. A residual LNAPL may also be found below the watertable after leaking from a deep underground storage tank or from a remnant watertable pool becoming trapped as the watertable rises.

The model includes a 3D, three-phase system (Fig. 2) consisting of a nonaqueous phase (the residual multi-component source), an aqueous phase (containing the dissolved diesel components and mobile carrier), and a sorbed phase (including the components and carrier which are sorbed to the aquifer solids). Conceptually, NAPL dissolution is assumed driven by the gradient between the effective solubility of a component at the NAPL surface and

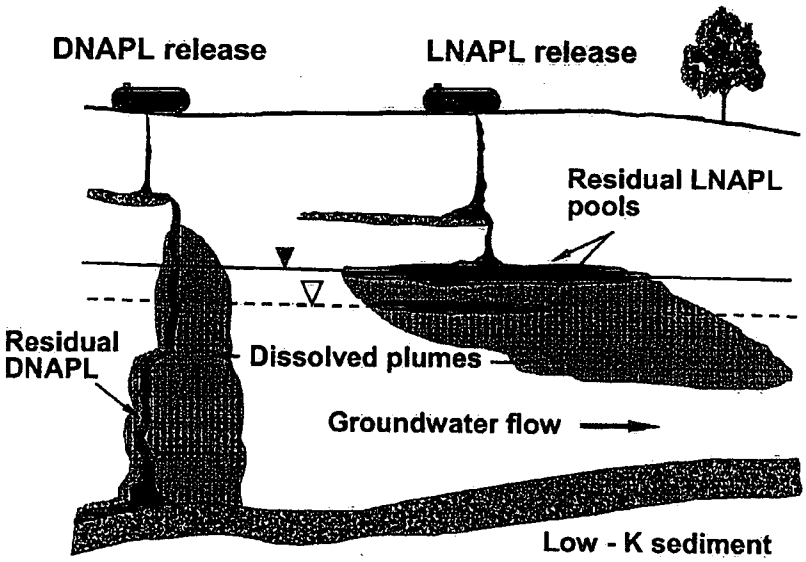

Fig. 1. Conceptual model for development of residual LNAPL or DNAPL sources within the saturated zone.

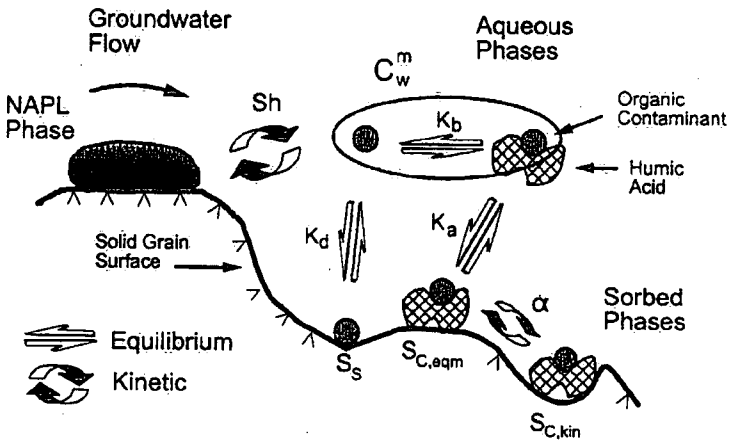

Fig. 2. Conceptual model for NAPL dissolution, solubilization and sorption to the organic carrier and solids. Here, C_w^m represents the aqueous pseudo-phase including both the free and carrier-bound organic.

its free aqueous concentration (Frind et al., 1999). As the free concentrations are reduced due to binding with the mobile carrier, the concentration gradient and dissolution rate increases.

Sorption of the diesel components to aquifer solids and to the mobile carrier is assumed instantaneous. Van Stempvoort and Lesage (2001b) show this is reasonable based on laboratory batch tests. Evidence for rapid binding of HOCs to humic acid is provided in McCarthy and Jiminez (1985) and Van Stempvoort and Lesage (in press). Sorption of the carrier and contaminant-bound carrier to the solids is represented by a mixed equilibrium/kinetic two-site model using Freundlich or Langmuir isotherms for the equilibrium component. The carrier is assumed to be in equilibrium with one fraction of the solid sorption sites while sorption to the remaining fraction follows the same isotherm but is kinetically limited. The approach combines the two-site sorption model used by Haggerty and Gorelick (1995) (extended here to include Langmuir isotherms) with the dissolution enhancement approach as presented by Ji and Brusseau (1998).

Key assumptions inherent in the conceptual model include: (1) the aquifer is saturated and non-fractured; (2) the NAPL phase is immobile; (3) the carrier is a single compound and carrier transport is unaffected by the presence of bound contaminants; (4) the mobile carrier phase does not degrade, and all phases sorbed to the solid do not degrade; (5) the contaminant degradation rates are not affected by binding to the mobile carrier; (6) the reaction stoichiometries assume complete degradation to CO_2 and H_2O; (7) the microbes are immobile and occupy limited pore space; and (8) inorganic geochemical processes (e.g. pH-dependent sorption) are not significant.

The study is limited to saturated systems because the experiment of Part 1 was designed to emulate a residual LNAPL trapped below the watertable. NAPL transport is not considered because the diesel source was at residual saturation and at field sites NAPL emplacement typically occurs on a time scale of days to weeks, whereas dissolution and aqueous transport may occur over years or decades. In this approach, only the *total*

contaminant concentration is transported (aqueous + "pseudo-phase" carrier-bound fractions, see Fig. 2), which is valid if the carrier is assumed governed by the same velocity field as the aqueous contaminants. Straining, in which the large HA molecules may become trapped in narrow or dead-end pores, is therefore not included. This approach is not a serious limitation since the use of NOM as a carrier is usually limited to medium or coarse-grained porous media where filtration effects would be minimal. The above assumptions are made to simplify the approach in light of the results from Part 1 of this series but may not be justified in other situations.

3.2. Governing equations for carrier transport

The general equation for reactive transport of a carrier can be expressed as:

$$\theta S_w \frac{\partial}{\partial x_i}\left(D_{i,j}\frac{\partial C_c}{\partial x_j}\right) - q_i\frac{\partial C_c}{\partial x_i} = \frac{\partial(\theta S_w C_c)}{\partial t} + f\rho_b\frac{\partial(S_c)}{\partial t} + (1-f)\rho_b\frac{\partial(S_{c,kin})}{\partial t} \quad (1)$$

where C_c (kg/m^3_w) is the aqueous carrier concentration, $D_{i,j}$ (m^2/s) is the hydrodynamic dispersion coefficient, q_i (m/s) is the Darcy flux, f is the mass fraction of sorption sites available for equilibrium sorption, S_w is the water saturation, ρ_b (kg/m^3) is the bulk density, θ is the porosity, t is time and x_i are the spatial coordinates. The sorbed phase carrier concentrations S_c and $S_{c,kin}$ represent the mass of carrier per mass of instantaneous and kinetically limited solid sorption sites, respectively.

S_c can be a linear or nonlinear function of the carrier concentration C_c. Assuming a Freundlich isotherm for example, the concentration of the carrier sorbed to the equilibrium sites can be written as:

$$S_c = K_a(C_c)^\eta \quad (2)$$

where K_a ($m^3_w/kg_{eqm\text{-}solids}$) is the sorption coefficient and η is a fitting parameter. If we assume a Langmuir-type isotherm for the equilibrium sorbed phase of the carrier, we can write:

$$S_c = QK_aC_c/(1+K_aC_c) \quad (3)$$

where Q ($kg_{carrier}/kg_{eqm\text{-}solids}$) is the maximum sorbed concentration for the equilibrium phase. The total sorbed phase carrier concentration S_T ($kg_{carrier}/kg_{total\text{-}solids}$) can be expressed as:

$$S_T = fS_c + (1-f)S_{c,kin} \quad (4)$$

Following the approach of Haggerty and Gorelick (1995), we express the kinetic sink term in Eq. (1) using

$$(1-f)\rho_b\frac{\partial(S_{c,kin})}{\partial t} = \rho_b\alpha[fS_c - (1-f)S_{c,kin}] \quad (5)$$

where α (s^{-1}) represents a first-order mass transfer coefficient between the equilibrium and kinetically sorbed carrier concentrations. The concentration of the carrier, which is kinetically sorbed to the aquifer solids, changes at a rate which is proportional to the difference in concentration between the equilibrium-sorbed phase and the kinetic-sorbed phase. Conceptually, this approach can represent kinetically limited intraparticle sorption, or grain surface-dependent sorption. In either case, it is gradient-driven mass transfer process. If the gradient on the right-hand-side of Eq. (5) is negative, a unique *desorption* rate coefficient α' can be used in place of α. For one-site sorption in which only equilibrium sorption of the carrier to solids is considered, we assign $\alpha = 0$.

Substituting Eq. (5) and either Eq. (2) or Eq. (3) into Eq. (1), dividing through by θS_w, and letting $\partial S_c/\partial t = (\partial S_c/\partial C_c)(\partial C_c/\partial t)$, the transport equation for the reactive carrier then becomes:

$$\frac{\partial}{\partial x_i}\left(D_{i,j}\frac{\partial C_c}{\partial x_j}\right) - v_i\frac{\partial C}{\partial x_i} = \frac{\partial (C_c)}{\partial t}R_1 + \frac{\rho_b \alpha}{\theta S_w}[f S_c - (1-f)S_{c,kin}] \tag{6}$$

where $v_i = q_i/\theta S_w$ and R_1 is the carrier retardation. Assuming a Langmuir isotherm, for example (Eq. (3)), we have:

$$R_1 = 1 + \frac{f\rho_b}{\theta S_w}\frac{QK_a}{(1+K_a C_c)^2} \tag{7}$$

During the solution of Eq. (6), the kinetically sorbed carrier concentration $S_{c,kin}$ is updated using Eq. (5) according to

$$S_{c,kin}^{t+\Delta t} = \frac{\alpha \Delta t}{(1-f)}(f S_c - (1-f)S_{c,kin}^t) + S_{c,kin}^t \tag{8}$$

where $S_{c,kin}^{t+\Delta t}$ and $S_{c,kin}^t$ are the sorbed concentrations at the new and old time step, respectively.

3.3. Governing equations for contaminant transport

The equation governing reactive transport of N_C dissolved phase components in the presence of a carrier (e.g. NOM) can be expressed, following the convention of Eq. (1), as:

$$\begin{aligned} &L(\theta S_w C_w^m) + \theta S_w\left[\lambda_{DIS}^m\left(C_s^m - \frac{C_w^m}{E^m}\right) - \lambda_{BIO}^m C_w^m\right] \\ &\quad = \theta S_w\frac{\partial (C_w^m)}{\partial t} + \rho_b\frac{\partial (S_{s-s}^m)}{\partial t} + \rho_b\frac{\partial (S_{s-c}^m)}{\partial t} \\ &m = 1, 2, \ldots N_C \end{aligned} \tag{9}$$

where $L(\theta S_w C_w^m)$ is an operator for advective–dispersive transport (equivalent to the left-hand side of Eq. (1)), C_w^m (kg/m^3) represents the *total* aqueous concentration of

component m (free + carrier-bound fractions), λ_{DIS}^{m} (s^{-1}) is the NAPL dissolution rate coefficient, λ_{BIO}^{m} (s^{-1}) is the biodegradation rate coefficient, C_s^m is the effective solubility, E^m is the solubility enhancement factor (described below), and $S_{s\text{-}s}^{m}$ and $S_{s\text{-}c}^{m}$ (kg/kg_{solid}) represent the concentrations of the contaminant sorbed to the aquifer solids and bound to the sorbed carrier, respectively. Following the terminology of Frind et al. (1999), the NAPL dissolution rate is expressed as

$$\lambda_{DIS}^{m} = Sh\frac{D^m}{(d_{50})^2} \tag{10}$$

where Sh is the Sherwood number, D^m (m^2/s) is the aqueous diffusion coefficient and d_{50} (m) is the mean grain size diameter. The Sherwood number Sh is a dimensionless coefficient which accounts for diffusive mass transfer within the NAPL, as well as effects of pore geometry and flow on the dissolution rate. It is often empirically defined as a function of the Reynolds number (see Frind et al., 1999; Imhoff et al., 1994).

In Eq. (9), the effective saturation of the NAPL component C_s^m is defined using Raoult's Law (modified to account for component activity), given as:

$$C_s^m = C_o^m X^m a^m \tag{11}$$

where C_o^m is the pure phase solubility (kg/m^3), X^m is the mole fraction and a^m is the activity coefficient of the component in the pure phase. Raoult's Law has been shown valid for predicting aqueous phase concentrations of diesel fuel components by Lee et al. (1992).

The biodegradation rate λ_{BIO}^{m} for component m in Eq. (9) can be expressed in terms of N_A parallel degradation reaction as

$$\lambda_{BIO}^{m} = \sum_{n=1}^{N_A}\left[k^{m,n}M^n\left(\frac{1}{K_C^{m,n}+C_w^m}\right)\left(\frac{A^n}{K_A^{m,n}+A^n}\right)I^n\right] \tag{12}$$

where N_A is the number of electron acceptors, $k^{m,n}$ ($kg_{HOC}/kg_{mic.}/day$) is the maximum utilization rate of component m with each electron acceptor, M^n ($kg_{mic.}/m_w^3$) is the concentration of the microbes associated with each electron acceptor, A^n is the concentration of electron acceptor n, $K_C^{m,n}$ and $K_A^{m,n}$ are the half utilization rate concentrations for the contaminant and electron acceptor, respectively, and I^n is the electron acceptor inhibition function.

In the case of multiple electron acceptors, the inhibition function (I^n) allows a transition between simultaneous or sequential consumption of electron acceptors. The function takes the form of

$$I^{n=1} = 1; \quad I^{n>1} = \prod_{i=2}^{n}\frac{1}{1+\dfrac{A^{i-1}}{K_I^{i-1}}} \tag{13}$$

where K_I^n represents the inhibition coefficient for electron acceptor n. In the case of oxygen and nitrate, for example, if $K_I^{O_2} = \varepsilon[O_2|_{max}]$, then setting $\varepsilon = 0.01$, for example, will

prevent utilization of nitrate until oxygen is nearly completely depleted. The approach follows that developed by Widdowson et al. (1988) and applied by Schäfer et al. (1998).

The electron acceptor concentration (A^n) in Eq. (12) is assumed to be dissolved in the aqueous phase, therefore transport is also assumed governed by advection and dispersion according to

$$\theta S_w \frac{\partial}{\partial x_i}\left(D_{i,j}\frac{\partial A^n}{\partial x_j}\right) - q_i\frac{\partial A^n}{\partial x_i} - \theta S_w \lambda^n_{BIO} A^n = \theta S_w \frac{\partial A^n}{\partial t} \qquad n = 1,2,\ldots N_A \quad (14)$$

where the electron acceptor rate term λ^n_{BIO} represents the net reaction rate due to biodegradation of all N_C components according to

$$\lambda^n_{BIO} = \sum_{m=1}^{N_C}\left[k^{m,n}M^n X^{m,n}\left(\frac{C^m_w}{K^{m,n}_C + C^m_w}\right)\left(\frac{1}{K^{m,n}_A + A^n}\right)I^n\right] \quad (15)$$

where $X^{m,n}$ represents the stoichiometric ratio of electron acceptor mass to contaminant mass.

After extending the approach of Frind et al. (1999) to account for multiple populations, microbial growth is calculated according to

$$\sum_{m=1}^{N_C}\left[Y^{m,n}M^n k^{m,n}\left(\frac{C^m_w}{K^{m,n}_C + C^m_w}\right)\left(\frac{A^n}{K^{m,n}_A + A^n}\right)I^n\right] - bM^n = \frac{\partial M^n}{\partial t} \quad (16)$$

where $Y^{m,n}$ is the yield coefficient ($kg_{mic.}/kg_{HOC}$) and b is a microbial decay rate (s^{-1}). One microbial population is coupled with each electron acceptor.

Following the approach of Ji and Brusseau (1998), the influence of a carrier on kinetic NAPL dissolution can be expressed in terms of an "enhancement factor" E^m which can be expressed as

$$E^m = 1 + K^m_b C_c \quad (17)$$

where K^m_b ($m^3_w/kg_{carrier}$) is the linear binding coefficient for the contaminant to the aqueous mobile carrier, and C_c is the mobile carrier concentration from Eq. (6).

Assuming a Freundlich isotherm, we can express the concentration of the contaminant which is sorbed to the aquifer solids as

$$S^m_{s-s} = K^m_d (C^m_w/E^m)^n \quad (18)$$

where K^m_d (m^3/kg_{solids}) is the linear distribution coefficient of component m between the aqueous and solid-sorbed phases. Assuming linear partitioning between the contaminant and carrier, the concentration of the contaminant which is sorbed to the sorbed carrier can be expressed as

$$S^m_{s-c} = \frac{K^m_b S_T C^m_w}{E^m} \quad (19)$$

where S_T is the total sorbed carrier concentration defined by Eq. (4).

Substituting Eqs. (18) and (19) into Eq. (9), and dividing through by θS_w, we obtain the general reactive transport equation:

$$\frac{\partial}{\partial x_i}\left(D_{i,j}\frac{\partial C_w^m}{\partial x_j}\right) - v_i\frac{\partial C_w^m}{\partial x_i} + \lambda_{DIS}^m\left(C_s^m - \frac{C_w^m}{E}\right) - \lambda_{BIO}^m C_w^m = \frac{\partial (C_w^m)}{\partial t}R_{eff}^m \tag{20}$$

where R_{eff} is the effective retardation coefficient which depends on the assumed sorption model. Assuming a Freundlich equilibrium model for sorption of the contaminant to the solids, and a two-site equilibrium/kinetic model for sorption of the carrier to solids, we have

$$R_{eff}^m = 1 + \frac{\rho_b K_d^m n (C_w^m)^{n-1}}{\theta S_w E^m} + \frac{\rho_b K_b^m}{\theta S_w E^m}[f(S_c^m) + (1-f)(S_{c,kin}^m)] \tag{21}$$

3.4. Numerical solution approach

Eq. (6) for the carrier, and Eqs. (20) and (14) for the contaminants and electron acceptors, are solved using a Galerkin finite element scheme using Picard iteration and deformable brick elements. The equations are coupled with Eq. (16) for microbial growth and decay. All nonlinear terms are centred in time and updated at each iteration. The Darcy flux q_i for the transport equations is obtained from a 3D groundwater flow algorithm iteratively coupled within the BIONAPL model (Frind et al., 1999).

Standard first-, second- and third-type (Cauchy) boundary conditions are available and convergence traps can be specified for the hydraulic head, HA carrier and HOC concentrations. The matrices are solved using a preconditioned conjugate gradient solver (Braess and König, 1995). Further details are provided by Molson (2000a,b).

4. Model evaluation

Earlier versions of the model incorporating either biodegradation or NAPL dissolution alone have previously been tested against analytical solutions (Schirmer et al., 1995), and calibrated to lab and field-scale experimental data (Frind et al., 1999; Knaus, 1999; Schirmer et al., 2000). The model has also been tested against a column experiment of humic acid-enhanced PCE solubilization (Molson, 2000b; using data from Johnson and John, 1999).

In this test, the numerical model is compared with a recently developed analytical solution for multiprocess nonequilibrium (MPNE; Neville et al., 2000). The evaluation includes four test problems including advective–dispersive transport with chemical nonequilibrium (two-site sorption), and first-order decay. In Section 6, the full model is tested through calibration of the pilot scale experiment.

The simulated column is 30 cm long with a first-type boundary concentration of 1.0 g/l applied over 9.7 days, then removed. For all cases, the porosity is 0.455, the Darcy flux is 0.03975 m/day, the bulk density is 1222 kg/m^3 and the dispersivity is 0.0061 m. Reactive

Table 1
Reactive transport parameters used in comparing the numerical BIONAPL model with the analytical MPNE model

Parameter	Value			
	Case 1	Case 2	Case 3	Case 4
Equilibrium distribution coefficient (K_d)	0.000426 m_w^3/kg	0.000426	0.000426	0.000426
Equilibrium mass fraction (f)	1.0 kg/kg	0.5	0.5	0.5
Sorption mass transfer coefficient (α)	0.0 day^{-1}	0.1	0.4	0.4
First-order decay coefficient (λ)	0.0 day^{-1}	0.0	0.0	0.069

parameters are provided in Table 1 which are based on experiments 1–4 used by Neville et al. (2000). Physical nonequilibrium is not considered in the examples here.

In the numerical model, the system was discretized with 50 elements and with a time step of 0.1 days. Results are shown as breakthrough curves at the outflow end of the column in Fig. 3. In Cases 1 and 2, the models include both one-site (equilibrium) and two-site (nonequilibrium) sorption. In Cases 3 and 4, the models assume two-site sorption for both a conservative (non-decaying) contaminant and for a contaminant with a half-life of 10 days for both the aqueous and solid-sorbed phases.

In all cases, the numerical and analytical solutions agree closely. Significant tailing is observed for Cases 2–4, which include two-site nonequilibrium sorption.

5. Description of the experiments

5.1. Sorption of humic acid to solids

Long-term (150-day) batch equilibrium experiments which studied sorption of humic acid to the aquifer solids (Van Stempvoort et al., 2000) clearly show a Langmuir-type

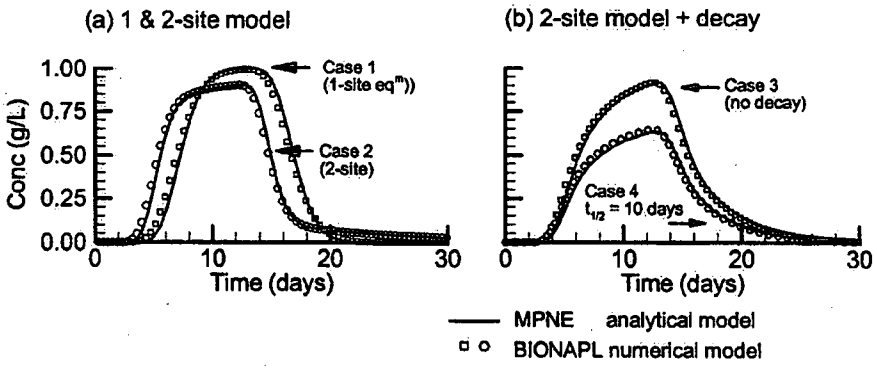

Fig. 3. Model evaluation: MPNE analytical model vs. BIONAPL numerical model for (a) one-site and two-site sorption, and (b) two-site sorption with and without decay.

isotherm from which best-fit parameters of $K_a = 39.1$ $m^3/kg_{eqm\text{-}solids}$ and $Q = 0.00042$ $kg_{HA}/kg_{eqm\text{-}solids}$ were obtained (Eq. (3) and Fig. 4). The data show that most sorption to the aquifer solids occurred at low aqueous HA concentrations from 0–0.2 kg/m^3, while at aqueous HA concentrations above 0.2 kg/m^3, there was relatively minor additional sorption. This behaviour is significant since at the high aqueous HA concentrations used here (approx. 0.83 kg/m^3), a greater proportion of the aqueous HA is available for binding with the aqueous contaminants. At lower aqueous HA concentrations, much of the HA is sorbed to the solids and may lead to *reduced* mobility of the contaminants as observed, for example, by Totsche et al. (1997). Further experimental data describing sorption of the contaminants and humic acid to the aquifer solids, and binding of the contaminants to the humic acid, are provided by Van Stempvoort and Lesage (2001a,b).

A significant kinetic component of HA sorption to aquifer solids was also observed in which an initial fast equilibrium sorption component is followed by a slow kinetically limited component (Fig. 5). This behaviour was reproduced with the two-site sorption model of BIONAPL using $\alpha = 0.005$ day^{-1} and $f = 0.47$. Approximately one-half of the solid sorption sites are therefore interpreted as being "fast" sites while the remainder are kinetically "slow". Kinetic sorption limitations have been attributed to intraparticle porosity or preferential sorption of relatively hydrophobic HA subcomponents (Magee et al., 1991; Vermeer et al., 1998).

5.2. The pilot scale experiment

The pilot scale enhanced remediation experiment was completed within a stainless steel tank measuring $5.5 \times 2.3 \times 2$ m in the longitudinal, transverse horizontal and vertical directions, respectively. The tank was filled with "Winter Sand" of porosity 0.30 and bulk density 1860 kg/m^3 (Van Stempvoort et al., this issue). One-half of the tank was used for the dissolution experiment (Fig. 6), while the other half was used for nonreactive control experiments. Approximately 500 ml of diesel fuel was mixed with 25 kg of water-wet

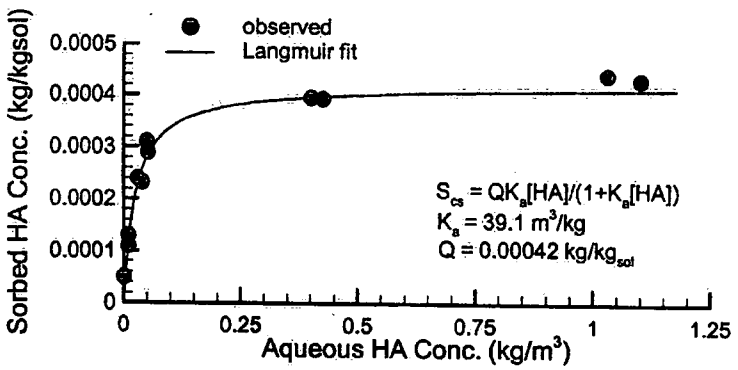

Fig. 4. Observed vs. fitted Langmuir isotherm for lab batch sorption test of humic acid to Winter Sand (after Van Stempvoort and Lesage, 2001b).

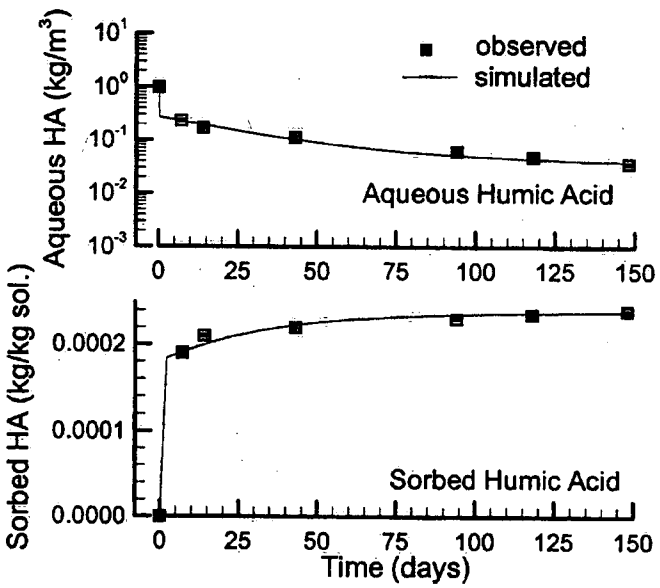

Fig. 5. Observed vs. simulated profiles showing early equilibrium and late kinetic sorption of humic acid to aquifer solids.

sand, creating an initial residual source with a NAPL saturation of approximately 0.09. Water and the humic acid solution entered from a head tank at the left, while effluent was withdrawn from a fully screened well located just inside the right boundary near the end of the tank.

The source was allowed to dissolve for 50 days under ambient conditions ($v \sim 2$ cm/h) after which humic acid was added to the head tank at a continuous concentration of 0.83 g/

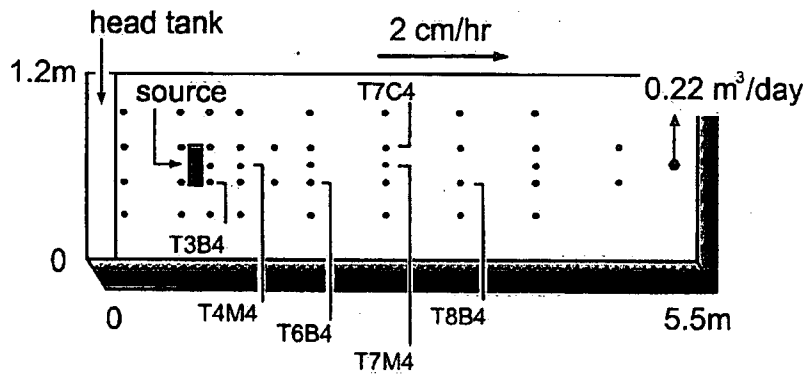

Fig. 6. Plan view of the pilot scale tank showing location of the source, monitor wells and extraction well. Selected monitor wells are mentioned in the text.

l and recirculated using the extraction well. Throughout the 5-year experiment, the dense 3D multilevel sampling array (Fig. 6) was monitored for humic acid and seven diesel components (BTEX, methyl-, dimethyl- and trimethylnaphthalene).

6. The pilot scale numerical model

6.1. Model parameters

The pilot scale model domain consisted of a three-dimensional grid measuring 5.5 × 1.2 × 1.25 m, resolved using 57 × 20 × 15 (=17,000) elements in the longitudinal, transverse horizontal and vertical dimensions, respectively (Fig. 7).

Grid spacing varied along the flow direction from 0.016 m within the source to 0.2 m towards the downgradient boundary. Spatial resolution was constrained by the grid Peclet criteria (Daus et al., 1985) and by reaction stability and convergence constraints. Simulation time steps varied from 0.2 days at early time and during initial HA flushing, to 1.0 days at later times.

Physical data for the pilot scale model are provided in Table 2. The flow velocity of 2 cm/h represents an average across the tank over the 5-year period. The initial velocity within the source during the dissolution experiment is approximately 15% lower because the residual diesel fuel is occupying pore space, which reduces the relative permeability. As the diesel fuel dissolves, the relative permeability increases and velocities within the source gradually recover to background levels. The flow system was constrained using a fixed head at the left inflow face (corresponding to the head tank) while all remaining boundaries were impermeable. Gradients were induced by the withdrawal well at the end of the tank.

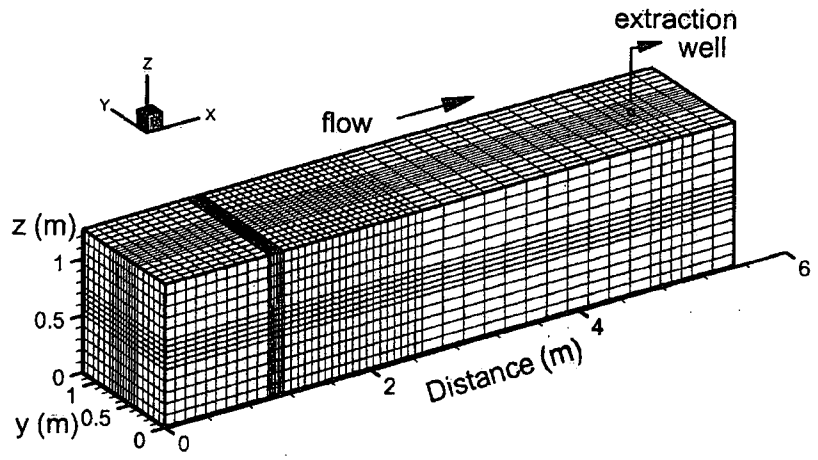

Fig. 7. Outline of the 3D finite element mesh for the pilot scale model. The residual diesel source is located at the intersection of the fine-mesh areas, 1.0 m from the inflow boundary.

Table 2
Flow system parameters used in simulating the pilot scale dissolution test

Parameter	Value	Source
Conductivity (K_x)	1.0×10^{-4} m/s	adjusted to fit initial velocity
Gradient (∇h)	0.0167	measured
Porosity (θ)	0.30	measured
velocity (v)	$\approx$2.0 cm/h[a]	Br tracer calibration
Bulk density (ρ_b)	1860 kg/m^3	measured
Median grain size (d_{50})	1.0 mm	measured
Dispersivity		
Longitudinal (α_L)	0.025 m	Br tracer calibration
Transverse horizontal (α_{TH})	0.005 m	Frind et al. (1999)
Transverse vertical (α_{TV})	0.005 m	Frind et al. (1999)

Measured data from Van Stempvoort et al. (this issue) and Van Stempvoort and Lesage (2001b).
[a] Represents the average velocity across the tank.

Seven unique diesel fuel components were considered in the model: benzene, toluene, ethylbenzene and the xylene isomers (BTEX), as well as methylnaphthalene (MN), dimethylnaphthalene (DMN) and trimethylnaphthalene (TMN) (collectively referred to here as methylated naphthalenes, or MNs). An eighth "pseudo-component" was used to represent the remaining, relatively less soluble, diesel fuel fraction (referred to here as "other" components). Oxygen was considered as the single electron acceptor with a single microbial population.

Physical properties assumed for the diesel fuel components are provided in Table 3. The binding coefficients K_b (for HOC to HA) for methyl- and dimethylnaphthalene are well

Table 3
Physical properties of the diesel fuel components assumed in the pilot scale model

Diesel component	ρ (kg/m^3)[a]	MW (kg/mol)[a]	C_o (kg/m^3)[a]	K_d [(m^3/kg) $\times 10^{-3}$][b]	K_b (m^3/kg)[c]	D^* [(m^2/s) $\times 10^{-10}$][d]
Benzene	876.6	0.078	1.78	0.0806	0.0	7.7
Toluene	870	0.092	0.515	0.161	0.0	6.6
Ethylbenzene	870	0.106	0.152	0.161	0.0	6.0
Xylenes	870	0.106	0.198	0.161	0.0	5.6
Methylnaphthalene	1000	0.142	0.035	0.20	2.1	6.6
Dimethylnaphthalene	1000	0.156	0.008	0.40	3.7	6.6
Trimethylnaphthalene	1000	0.170	0.0021	1.3	10.0	6.6
Other compounds	862	0.230	0.001	1.3	10.0[e]	5.0

[a] From Wiedemeier et al. (1999) and CRC Handbook (1980). Data for "other compounds" were derived from average diesel fuel properties.
[b] BTEX K_d values chosen to yield $R_{benzene} = 1.5$, and $R_{TEX} = 2.0$ (see Wiedemeier et al., 1999); MN K_d values derived from laboratory data (Van Stempvoort and Lesage, 2001b).
[c] From Van Stempvoort and Lesage (2001a), and adjusted during calibration. BTEX sorption to HA assumed negligible. Note: K_b is defined here as m^3/kg$_{HA}$ (=l/g$_{HA}$); to compare with Van Stempvoort et al. (this issue, Table 6—$K_{oc,app}$ in l/kg$_{Carbon}$), multiply $K_{oc,app}$ by 0.00036 (=0.000301 kg$_C$/0.83 g$_{HA}$).
[d] From Wiedemeier et al. (1999, Appendix B), assuming a tortuosity of 0.7.
[e] Assumed at least equal to K_b for trimethylnaphthalene; no data available.

within the range of lab data from Van Stempvoort et al. (this issue); however, the model-derived value for K_b^{TMN} is somewhat higher than the lab-derived value. The difference is attributed to different binding coefficients among several TMN isomers, which were not considered in the lab experiment or model.

Additional parameters pertaining to the diesel fuel source are provided in Table 4. Mass estimates were obtained from laboratory data and from cumulative flux calculations based on the observed breakthrough data (Van Stempvoort et al., this issue). The mass of the remaining, unknown components is then computed based on assuming an average molecular weight for diesel fuel of 0.230 kg/mol, an average density of 1000 kg/m^3, and a source volume of 500 ml.

The Sherwood number, which controls the diesel dissolution rate, was unknown and had to be calibrated using the observed breakthrough data of each component. In a controlled field experiment of a dissolving solvent mixture, Frind et al. (1999) found good agreement with previously published trends which showed the Sherwood number decreasing with the Reynolds number. In the current study, the Reynolds number is on the order of 4×10^{-3} and the range of calibrated Sherwood numbers (0.9–2.2) is consistent with data provided by Powers et al. (1994). Activity coefficients for the MNs were also calibrated using the observed breakthrough data, and agree well with published data based on synthetic jet fuel mixtures (Burris and MacIntyre, 1987).

Biodegradation parameters were either calibrated or obtained from the literature (e.g. Schirmer et al., 2000; Bekins et al., 1998). Maximum utilization rates (k^m) for BTEX were fixed at 0.5 $kg_{HOC}/kg_{mic.}$/day and maximum rates were calibrated to 0.02 $kg_{HOC}/kg_{mic.}$/day for the MNs, and to 0.20 $kg_{HOC}/kg_{mic.}$/day for the "other" components. The half-saturation constants (K_C and K_A) were fixed at 2.0 mg/l to be consistent with previous estimates. The microbial yield coefficient (Y) for all components was fixed at 0.5 $kg_{mic.}/kg_{org}$, and was applied under the assumption that the biomass carbon is not a significant fraction of the mineralized carbon. The oxygen/substrate mass stoichiometry ratios are

Table 4
Characterization of the simulated diesel fuel source

Diesel component	Source Mass (kg)[a]	Moles	Mole fraction	Sh[b]	Activity coefficient[c]
Benzene	4.7e−6	6.0e−5	0.000028	1.0	1.0
Toluene	1.8e−4	0.002	0.000095	2.0	1.0
Ethylbenzene	5.3e−4	0.005	0.00237	1.0	1.0
Xylenes	1.1e−3	0.01	0.00475	1.0	1.0
Methylnaphthalene	0.001	0.007	0.00332	0.9	1.5
Dimethylnaphthalene	0.005	0.032	0.0152	0.9	2.1
Trimethylnaphthalene	0.005	0.029	0.0138	2.2	2.1
Other compounds	0.465	2.022	0.9596	2.2	2.0
Total	0.478	2.107	1.0		–

[a] Van Stempvoort et al. (accompanying paper), Table 4.
[b] Calibrated Sherwood number (see Eq. (10)).
[c] Calibrated for MNs.

calculated assuming complete mineralization. Mineralization of methylnaphthalene, for example, can be written as:

$$C_{11}H_{10} + \frac{27}{2}O_2 \Rightarrow 11CO_2 + 5H_2O \quad (22)$$

where the oxygen/substrate mass ratio is 3.04. Mass ratios for the eight diesel components ranged from 3.04 to 3.20. Boundary input and initial background oxygen concentrations were assumed to be 6.0 mg/l, correlating with background tank measurements. The initial microbe concentration was fixed at 5.0 mg/l and microbes were not allowed to grow beyond 14 mg/l to prevent pore clogging. The microbial decay coefficient (b) was 10^{-10} s^{-1}.

6.2. Transport of humic acid

The humic acid carrier was added to the tank 51 days after source emplacement at a concentration of 0.83 g/l. The observed vs. simulated breakthrough curves of the humic acid at monitor well T3B4 and T7C4 are provided in Fig. 8.

The carrier arrived at the two respective monitor wells approximately 5 and 10 days following addition to the head tank. The arrival curves are steep until the concentration reaches about 0.5 g/l, after which nonlinear kinetic sorption of the carrier to aquifer solids induces significant tailing. For this simulation, only the kinetic sorption rate coefficient had to be calibrated ($\alpha = 0.05$ day^{-1}), the remaining parameters (K_a, Q, f) were obtained

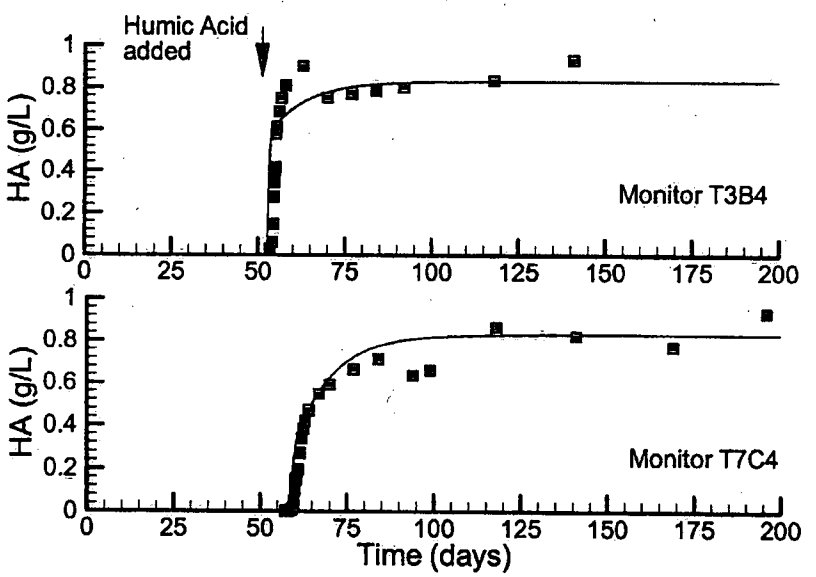

Fig. 8. Simulated vs. observed breakthrough of the humic acid carrier in the pilot scale experiment at monitors T3B4 (top) and T7C4 (bottom).

independently from batch experiments (Table 5). Simulations using the lower batch-calibrated rate of 0.005 day^{-1} (not shown) induced a steep arrival curve with almost no tailing and clearly did not match the observed behaviour.

The reason for the discrepancy between the sorption rate coefficient for the batch experiment (0.005 day^{-1}) and that fitted at the pilot scale (0.05 day^{-1}) is not clear. The dynamic nature of the pilot scale experiment and the effect of mixing over the discrete elements is likely important.

6.3. Transport of the diesel components

Among the eight diesel fuel components included in the model, the four BTEX components were the most soluble and completely dissolved from the source within 100 days (Van Stempvoort et al., this issue). Because of their high solubility, there was no observed effect of the humic acid on these components. We will therefore focus the discussion on the MN components instead.

The (total) MN plumes are shown in plan view (through the source centre) at 41, 70, 385, 958 and 1380 days in Fig. 9a and b for the observed and simulated systems, respectively. At 41 days (10 days before adding humic acid), the simulated plume has attained a steady state configuration with source concentrations of about 400 μg/l. Also, the outermost 50 μg/l contour has just reached the extraction well, which is in good agreement with the observed plume. At 70 days (19 days after adding humic acid), the source concentration has increased to 1700 μg/l due to humic acid-enhanced solubilization of the residual diesel. The simulated 50 μg/l contour, however, has somewhat receded relative to its location at 41 days (Fig. 9b).

The apparent shortening of the simulated plume is caused by enhanced sorption in which the carrier-bound contaminants become sorbed to the aquifer solids. Fig. 10 shows the total MN plumes and corresponding humic acid profiles at 55 and 65 days. At 55 days, for example, the humic acid front is located approximately 1.5 m from the head tank. The profile is asymmetric because of the nonlinear Langmuir isotherm and the slow kinetic component of the two-site sorption model. The HA front correlates with the low-concentration break in the MN plume where enhanced sorption has decreased the concentrations of the aqueous diesel components. By 65 days (14 days after adding HA), the HA front has advanced to about 4 m. Dispersion of the humic acid causes the

Table 5
Humic acid sorption parameters assumed in the pilot scale simulation model

Parameter	Value	Source
Binding coefficient: HA-solids (K_a)	39.1 $m^3/kg_{eqm\text{-}solids}$	Langmuir fit to batch data[a]
Maximum sorbed concentration: HA-solids (Q)	0.00042 $kg_{HA}/kg_{eqm\text{-}solids}$	Langmuir fit to batch data[a]
Sorption mass transfer coefficient (α)	0.05 day^{-1}	calibrated to pilot scale HA breakthrough
Fraction of equilibrium sites (f)	0.47	calibrated from kinetic batch data

[a] Van Stempvoort et al. (2000).

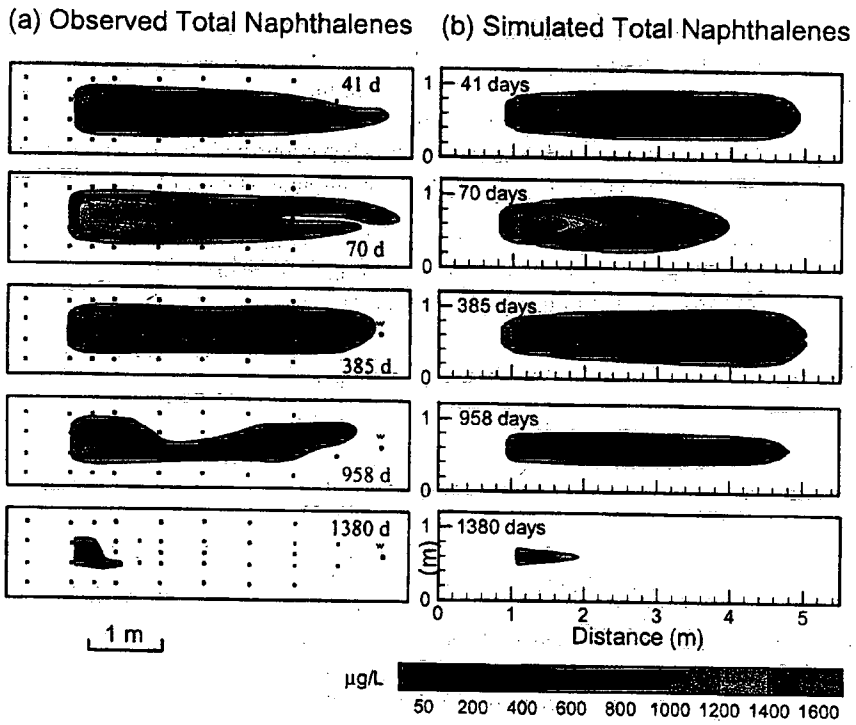

Fig. 9. Total methylated naphthalene plumes at selected times showing (a) observed data from the pilot scale experiment and (b) results from the numerical simulation. Plumes are shown in plan view through source centre. Observed data from Van Stempvoort et al. (this issue).

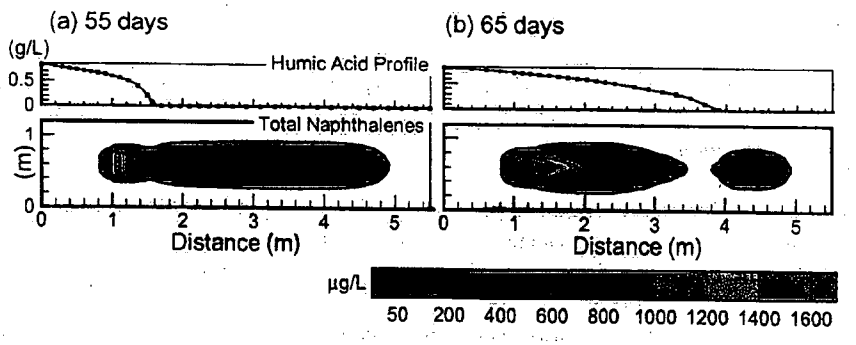

Fig. 10. Simulated total methylated naphthalene plumes at (a) 55 and (b) 65 days showing corresponding humic acid profiles. Contour plots are plan view, located through the source centre.

MN depression to widen, and by 65 days, the 50 μg/l contour of the main plume has separated completely from the advanced lobe. Once the carrier reaches higher concentrations along the plateau of the Langmuir isotherm, the sorption sites become saturated and the carrier-bound contaminants are no longer retarded. The MN plume then begins to re-advance. No attempt was made to correlate this behaviour with the observed distribution; however, it was observed in some of the breakthrough data as a brief concentration drop after arrival of the humic acid (Fig. 11).

By 385 days, the total MN plume has re-advanced although concentrations have already begun to decrease due to source depletion and biodegradation (Fig. 9). By 958 days, the plume has receded to the extent that the 50 μg/l contour no longer reaches the extraction well. After 1380 days, the source concentration has decreased to approximately 200 μg/l and the plume extends less than a metre from the source. The simulated plumes clearly do not match the observed small-scale irregularities; however, the general pattern and concentration levels are maintained.

The simulated breakthrough curves of the methylated naphthalene components at a point immediately downgradient from the source (monitor T3B4) are compared to the observed data in Fig. 11. During the initial 50-day period before humic acid was added, the diesel source was being flushed only by water. The component concentrations reach equilibrium levels which, through Raoult's Law, depend on their aqueous solubilities, mole fractions and activities. Shortly after the humic acid was added, binding of the MNs onto the humic acid rapidly increased their effective solubilities with the steepest rise occurring within 5 days of the humic acid arrival (Fig. 11). Due to enhanced sorption, peak enhanced solubilities were not reached until somewhat later. For the methylnaphthalenes, the peak occurred 15 days after arrival of the humic acid, 30 days later for the dimethylnaphthalenes, and 45 days later for the trimethylnaphthalenes. As the humic acid front passed the source, the humic acid concentrations reached the plateau of the Langmuir isotherm and the maximum enhanced solubility was reached.

The solubilities of the diesel components increased by up to a factor of 10 for the trimethylnaphthalenes, and by factor of 5 and 2 for the dimethylnaphthalenes and methylnaphthalenes, respectively. After reaching the maximum solubility, concentrations slowly decline due to source mass depletion and biodegradation. The simulations suggest that the source was dissolving at equilibrium or near-equilibrium conditions throughout the experiment. The predicted dissolution times to reduce aqueous concentrations to 10 μg/l (representing a typical drinking water limit) were 500, 1200 and 1700 days for the methyl-, dimethyl- and trimethylnaphthalenes, respectively (Fig. 11).

6.4. Biodegradation

Throughout the experiment, biodegradation of the source and dissolved diesel components was active. Supporting evidence came from measured background oxygen concentrations on the order of 6.5 to 8.5 mg/l, while oxygen data within the dissolved plume ranged from 0.03 to 2.98 mg/l, with most concentrations less than 0.5 mg/l (Van Stempvoort et al., this issue). Oxygen was clearly being depleted; however, the specific spatial and temporal variation was unavailable. Simulated oxygen depletion plumes are provided in Fig. 12a for 41–385 days, which show oxygen-limiting conditions developing within the

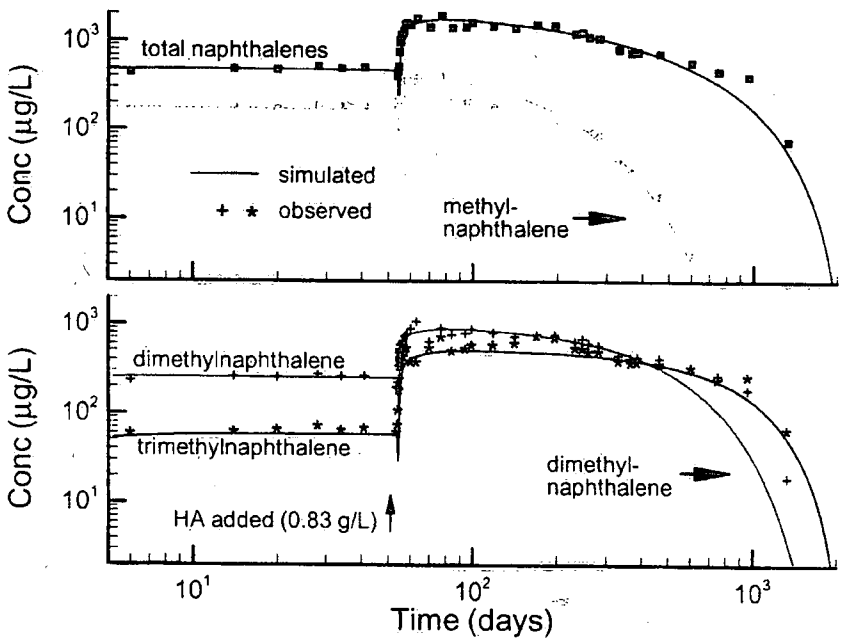

Fig. 11. Observed vs. simulated breakthrough of the naphthalene components at monitor well T3B4 (immediately downgradient from the source).

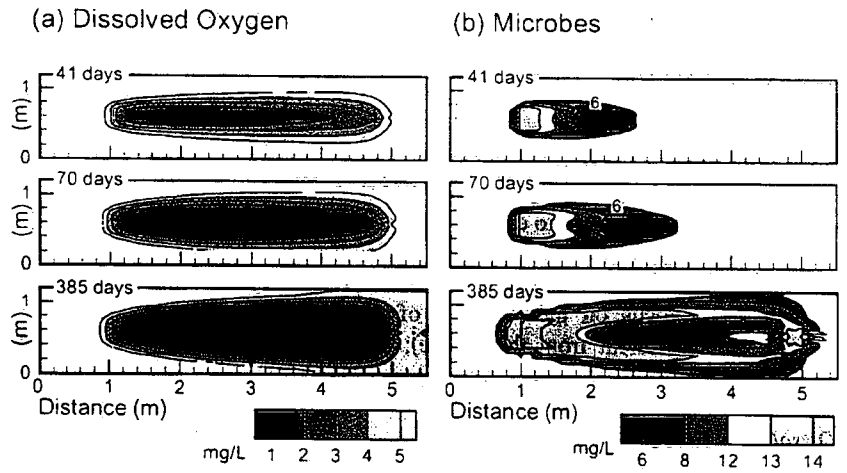

Fig. 12. Simulated plumes of (a) oxygen depletion and (b) microbial growth caused by biodegradation of the diesel fuel components. The images represent horizontal slices through the source centre at selected times. Oxygen contours are only flooded for depleted areas with less than the background concentration of 6 mg/l.

core of the contaminant plumes. By 385 days, the distribution of dissolved oxygen has reached steady state and depletion is maintained by biodegradation of the (unmonitored) remaining diesel fraction. Because of rapid upgradient replenishment, the lowest oxygen concentrations are not found within the source, but are located downgradient, close to the extraction well where biodegradation rates are high due to rapid mixing.

The simulated depletion of oxygen was accompanied by higher microbe concentrations, especially within the mixing zones where contaminant and oxygen concentrations are both sufficiently high to sustain growth (Fig. 12b). At early time, the microbes grow rapidly within the source where contaminant concentrations remain high and oxygen-rich water arrives from upgradient. By 385 days, the microbes have formed a shell of elevated concentrations, which correlates with the mixing zone surrounding the organic plumes. Somewhat higher concentrations are also found at the extraction well where enhanced mixing favours microbial growth. Microbe concentrations within the centre of the contaminant plumes remain at minimum levels because of almost complete oxygen depletion and natural microbial decay. Since observed microbial mass data were limited, quantitative comparisons were not attempted at this stage of the modeling and will be left for future study.

The simulated microbial growth pattern suggests some interesting possibilities for explaining observed trends in the methylated naphthalene concentrations that were not reproduced in the model. The observed low MN concentrations down the plume centreline, for example, could be a result of the flow field bypassing the biomass-clogged source. The decrease in relative permeability due to the presence of residual diesel (included in the model) is not sufficient to account for this trend. Also, the observed drop in the breakthrough concentrations at several monitor wells could be due to small transients in the flow field, again perhaps caused by microbial growth and decay. Because of the high concentration gradients, a small lateral shift in the plume, on the order of a few centimetres, would be sufficient to cause the observed trend. To simulate these effects, the model could be modified to include coupling between the microbial mass and the relative permeability.

7. Sensitivity analysis

A sensitivity analysis is used to explore the influence of several parameters which were calibrated or showed measurement uncertainty. In each of the following cases, only the parameters for the MNs were changed, the corresponding BTEX parameters were held constant. We will focus on the response of trimethylnaphthalene at monitor T3B4 (immediately downgradient from the source); the responses were similar for MN and DMN.

7.1. Dissolution rate

To investigate the influence of the dissolution rate in the pilot scale experiment, the model was run using Sherwood numbers of one-tenth and 10 × those calibrated for the MNs (Table 4). The results are compared to the model calibration for TMN at monitor

T3B4 in Fig. 13a which illustrates that the lower dissolution rate significantly reduces the breakthrough concentrations, even after the humic acid carrier arrives. The early-time (0–50 days) observed concentration plateaus are now underestimated and there is significantly more tailing in the breakthrough profiles resulting in much longer dissolution times. Increasing the dissolution rate by a factor of 10, however, has very little influence on the breakthrough concentrations, which suggests that the diesel fuel was dissolving under equilibrium or near-equilibrium conditions. Some degree of non-uniqueness must be acknowledged here, since the breakthrough response using a lower dissolution rate would be similar to that of a lower HOC–HA binding coefficient.

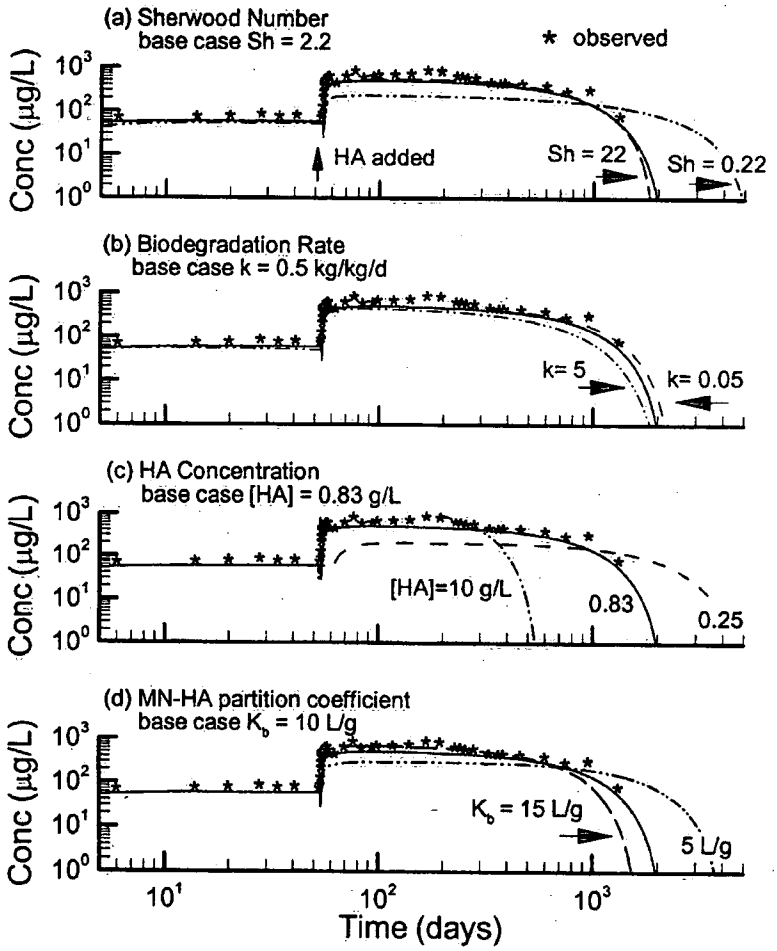

Fig. 13. Model sensitivity to (a) dissolution rate, (b) max. biodegradation rate, (c) HA concentration and (d) MN–HA partition coefficient. Results shown for TMN at monitor T3B4, base case simulations shown as solid line.

7.2. Biodegradation rate

The maximum biodegradation rate (k^m in Eq. (12)) was not independently known for the pilot scale experiment and had to be calibrated based on the observed breakthrough curves. The sensitivity of the TMN component concentrations to k^m is provided in Fig. 13b (recall k^m was concurrently increased for MN, DMN and the remaining diesel fraction). With the rate increased by a factor of 10, the concentrations decreased only slightly relative to the base case because the system was oxygen-limiting. Decreasing the rate also had a limited effect because this monitor is close to the source. At points further downgradient, biodegradation was somewhat more apparent in the breakthrough curves. The effect of the biodegradation rate is clearly distinguishable from that of the dissolution rate. While increasing the biodegradation rate reduces the concentrations throughout the observation period, decreasing the dissolution rate only reduces the early-time concentrations, and causes significant tailing (relatively higher concentrations) at longer times.

7.3. Carrier concentration

The concentration of a reactive carrier directly influences the degree of solubilization of a residual NAPL through the enhancement factor (Eq. (17)). Although high carrier concentrations will increase solubilization, sorption to aquifer solids at low carrier concentrations may reduce the mobility of the dissolved phase contaminants. Here, the sensitivity of the diesel fuel dissolution is tested with respect to the humic acid carrier concentration. The HOC–HA binding coefficients (K_b) remain the same as in the calibration simulation.

Simulations of the pilot scale experiment ([HA] = 0.83 g/l) were repeated with humic acid concentrations of 0.25 and 10 g/l, and results compared with the experimental and calibrated results in Fig. 13c. The 0.25 g/l concentration was chosen as it lies at the breakpoint of the Langmuir isotherm (Fig. 4), and Johnson and John (1999) use humic acid concentrations up to 12 g/l in their experiments. The results show a high sensitivity to the carrier concentration as would be expected from the corresponding enhancement factor ($E = 1 + K_b[HA]$). Decreasing the carrier concentration to 0.25 g/l, for example, increases the time for complete dissolution of trimethylnaphthalene (to 10 μg/l) by 112%, while increasing the concentration to 10 g/l reduces the time by 71%.

7.4. Binding coefficient: HOC–HA

The binding coefficient (K_b) describes the tendency for the HOCs to bind to the mobile humic acid. For the base case (calibration) simulation, values of K_b were obtained from lab-derived data provided by Van Stempvoort et al. (this issue), and listed here in Table 3. Among the three MN components, the most significant variation and uncertainty was observed for trimethylnaphthalene because of the greater number of isomers, of which only one was tested (2,3,5-TMN). Since trimethylnaphthalene is also the least soluble of the three components, its binding coefficient had the greatest effect on the bulk dissolution rate.

To determine the sensitivity of the model to the binding coefficient of trimethylnaphthalene, the base simulation was repeated for two different values of K_b^{TMN}, while keeping K_b^{MN} and K_b^{DMN} unchanged. The results are provided in Fig. 13d. The range of K_b was selected based on estimated uncertainty in the observed data. Reducing the coefficient from 10 l/g in the base simulation to 5 l/g clearly does not match the observed data and significantly increases the time for complete dissolution. Increasing the coefficient from 10 to 15 l/g provides a somewhat improved match at early time (51–500 days), but slightly underestimates the total dissolution time. The effect of changing the binding coefficient of TMN had a negligible effect on the behaviour of MN and DMN (not shown).

7.5. Long-term dissolution

In the absence of a carrier, the diesel source will dissolve more slowly and the effective biodegradation rate will be reduced since the total aqueous phase organic concentrations are lower. This behaviour is shown in Fig. 14 in which the rate of source mass depletion from the carrier-enhanced model is compared to an otherwise equivalent simulation assuming no carrier. The results show that the humic acid carrier has decreased the time required to deplete the source by a factor of about 2 for methylnaphthalene, 4 for dimethylnaphthalene, and 6 for trimethylnaphthalene and the remaining components. Although the enhancement factors for the remaining components

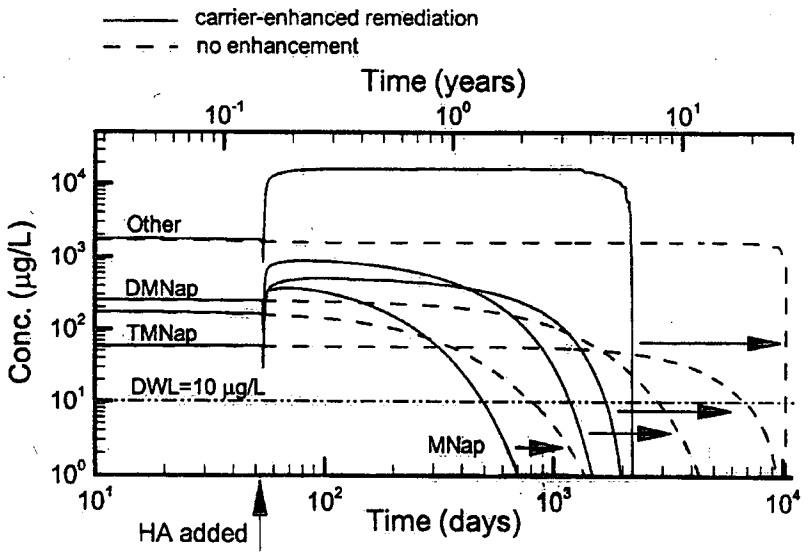

Fig. 14. Long-term dissolution of the diesel fuel source: comparison at monitor T3B4 between the calibrated, humic acid-enhanced model, and an equivalent simulation without a carrier. Arrows indicate shift from the carrier-enhanced simulation to the no-enhancement simulation.

were unknown ($K_b^{\text{other cpds.}}$ is assumed constant at 10 l/g—see Table 3), both the observed and simulated sources were almost completely dissolved and degraded after 5 years; hence, we can be confident of the simulated bulk dissolution behaviour for the unknown fraction. The reduction in dissolution time is not identical to the enhancement factors because of kinetic dissolution limitations, and because of nonlinear sorption and biodegradation.

8. Conclusions

The processes required to simulate humic acid-enhanced remediation of diesel fuel include groundwater flow, multi-component NAPL dissolution, solubilization and transport of the diesel components, and transport of humic acid. The observed data show that a two-site (instantaneous and kinetically limited) model was required to simulate sorption of humic acid to the aquifer solids. Linear equilibrium sorption of the contaminants to solids and contaminants to humic acid carrier was shown sufficient to reproduce the observed MN plumes and breakthrough curves. The simulations confirmed the observed 10-fold increase in apparent solubility of trimethylnaphthalene, with increases on the order of 2–5 for the methyl- and dimethylnaphthalenes.

Simulated depletion plumes of dissolved oxygen followed the observed trends with almost complete oxygen depletion within the core of the diesel component plumes. Most biodegradation seemed to be maintained by the remaining, unmonitored fraction of the diesel components, while degradation of the methylated naphthalenes, at least near the source, appeared to be minimal. Permeability reductions due to biomass could explain some of the observed trends in the methylated naphthalene concentrations that were not reproduced by the model. The decrease in relative permeability due to the residual diesel was not sufficient to cause significant flow bypassing.

A sensitivity analysis of the effective dissolution rate suggested that the methylated naphthalenes within the diesel source were dissolving at or near equilibrium throughout most of the 5-year observation period. Because of oxygen limitations, the solution appeared relatively less sensitive to the maximum biodegradation rate (k^m).

The humic acid source concentration in the experiment was fixed at 0.83 g/l, which almost completely dissolved the source within 5 years. Increasing the HA concentration to 10 g/l reduced the simulated dissolution time by up to 71% for trimethylnaphthalene, while a decrease to 0.25 g/l more than doubled the required dissolution time. Predictive simulations suggest that complete dissolution of the methylated naphthalene components in the pilot scale test would take up to six times longer without the humic acid carrier. The time required for complete remediation (to drinking water limits) of the complete diesel fuel source was limited by the degree of solubilization of the remaining unknown diesel components.

The benefits of using humic acid, both physical and economic, must be compared with those of surfactants and other remediation alternatives before a suitable remediation approach is chosen for a specific site. Full field-scale experiments and simulations would confirm remediation efficiency and help identify further limitations.

Acknowledgements

We thank Chris Neville for supplying the MPNE analytical solution for two-site sorption, and Mario Schirmer for helpful contributions. We are grateful for the thorough review provided by William P. Johnson, as well as comments from an anonymous reviewer. This study was supported in part by an NSERC grant to the second author, and a contribution from CRESTech. The authors also wish to thank the Panel for Energy Research and Development (PERD), the National Energy Board and Environment Canada for their support.

References

Abdul, A.S., Gibson, T.L., Rai, D.N., 1990. Use of humic acid solution to remove organic contaminants from hydrogeologic systems. Environ. Sci. Technol. 24, 328–333.

Bekins, B., Warren, E., Godsy, E.M., 1998. A comparison of zero-order, first-order and Monod biotransformation models. Groundwater 36 (2), 261–268.

Boving, T.B., Brusseau, M.L., 2000. Solubilization and removal of residual trichloroethene from porous media: comparison of several solubilizing agents. J. Contam. Hydrol. 42 (1), 51–67.

Braess, D., König, C., 1995. A fast conjugate gradient algorithm for three dimensional groundwater flow problems. Ruhr-Universität Bochum.

Brusseau, M.L., McCray, J.M., Johnson, G.R., Wang, X., Wood, A.L., Enfield, C., 1999. Field test of cyclodextrin for enhanced in-situ flushing of multiple-component immiscible organic liquid contamination: project overview and initial results. Chapter 9. In: Brusseau, M.L., Sabatini, D.A., Gierke, J.S., Annable, M.D. (Eds.), Innovative Subsurface Remediation: Field Testing of Physical, Chemical, and Characterization Technologies. American Chemical Society, Washington, DC.

Bryan, N.D., Robinson, V.J., Livens, F.R., Hesketh, N., Jones, M.N., Lead, J.R., 1997. Metal–humic interactions: a random structural modelling approach. Geochim. Cosmochim. Acta 61 (4), 805–820.

Burris, D.R., MacIntyre, W.G., 1987. Water solubility behavior of hydrocarbon mixtures—implications for petroleum dissolution. In: Vandermeulin, H., Hrudey, S. (Eds.), Oil in Freshwater: Chemistry, Biology, Countermeasures Technology. Symposium of Oil Pollution in Freshwater, Edmonton, Canada. Pergamon Press, New York, pp. 85–94.

Chiou, C.T., Kile, D.E., Brinton, T.I., Malcolm, R.L., Leenheer, J.A., MacCarthy, P., 1986. A comparison of water solubility enhancements of organic solutes by aquatic humic materials and commercial humic acids. Environ. Sci. Technol. 21 (12), 1231–1234.

Corapcioglu, M.Y., Jiang, S., 1993. Colloid-facilitated groundwater contaminant transport. Water Resour. Res. 29 (7), 2215–2226.

Corapcioglu, M.Y., Kim, S., 1995. Modeling facilitated contaminant transport by mobile bacteria. Water Resour. Res. 31 (11), 2639–2647.

CRC Handbook, 1980. CRC Handbook of Chemistry and Physics. CRC Press, Boca Raton, Florida.

Danzer, J., Grathwohl, P., 1998. Coupled transport of PAH and surfactants in natural aquifer material. Phys. Chem. Earth 23 (2), 237–243.

Daus, A.D., Frind, E.O., Sudicky, E.A., 1985. Comparative error analysis in finite element formulations of the advection–dispersion equation. Adv. Water Resour. 8, 86–95.

Frind, E.O., Molson, J.W., Schirmer, M., Guiguer, N., 1999. Dissolution and mass transfer of multiple organics under field conditions: the Borden source. Water Resour. Res. 35 (3), 683–694.

Grimberg, S.J., Stringfellow, W.T., Aitken, M.D., 1996. Quantifying the biodegradation of phenanthrene by *Pseudomonas stutzeri* P16 in the presence of a non-ionic surfactant. Appl. Environ. Microbiol. 62 (7), 2387–2392.

Grubb, D., Sitar, N., 1999. Mobilization of trichloroethene (TCE) during ethanol flooding in uniform and layered sand packs. Water Resour. Res. 35 (11), 3274–3283.

Guetzloff, T.F., Rice, J.A., 1994. Does humic acid form a micelle? Sci. Total Environ. 152, 31–35.
Guha, S., Jaffe, P.R., 1996. Biodegradation kinetics of phenanthrene partitioned into the micellar phase of non-ionic surfactants. Environ. Sci. Technol. 30 (2), 605–611.
Haggerty, R., Gorelick, S.M., 1995. Multiple-rate mass transfer for modeling diffusion and surface reactions in media with pore-scale heterogeneity. Water Resour. Res. 31 (10), 2383–2400.
Hunter, K.S., Wang, Y., Cappellan, P.V., 1998. Kinetic modelling of microbially-driven redox chemistry of subsurface environments: coupling transport, microbial metabolism and geochemistry. J. Hydrol. 209, 53–80.
Ibaraki, M., Sudicky, E.A., 1995. Colloid-facilitated contaminant transport in discretely-fractured porous media: 1. Numerical formulation and sensitivity analysis. Water Resour. Res. 31 (12), 2945–2960.
Imhoff, P.T., Jaffe, P.R., Pinder, G.F., 1994. An experimental study of complete dissolution of a nonaqueous phase liquid in saturated porous media. Water Resour. Res. 30 (2), 307–320.
Jardine, P.M., Dunnivant, F.M., Selim, H.M., McCarthy, J.F., 1992. Comparison of models describing the transport of dissolved organic carbon in aquifer columns. Soil Sci. Soc. Am. J. 56, 437–444.
Ji, W., Brusseau, M.L., 1998. A general mathematical model for chemical-enhanced flushing of soil contaminated by organic compounds. Water Resour. Res. 34 (7), 1635–1648.
Johnson, W.P., 2000. Sediment control of facilitated transport and enhanced desorption. J. Environ. Eng. 126 (1), 47–56.
Johnson, W.P., John, W.W., 1999. PCE solubilization and mobilization by commercial humic acid. J. Contam. Hydrol. 35, 343–362.
Johnson, W.P., Amy, G.L., Chapra, S.C., 1995. Modelling of NOM-facilitated PAH transport through low-foc sediment. J. Environ. Eng. 121 (6), 438–446.
Knabner, P., Totsche, K.U., Koegel-Knabner, I., 1996. The modeling of reactive solute transport with sorption to mobile and immobile sorbents: 1. Experimental evidence and model development. Water Resour. Res. 32 (6), 1611–1622.
Knaus, M., 1999. Modellsimulationen zur Freisetzung von Schadstoffen aus kohärenter Flüssigphase. Diplomarbeit, Eberhard-Karls-Universität Tübingen.
Lee, L.S., Hagwall, M., Delfino, J.J., Rao, P.S., 1992. Partitioning of polycyclic aromatic hydrocarbons from diesel fuel into water. Environ. Sci. Technol. 26, 2104–2110.
Lesage, S., Xu, H., Novakowski, K.S., Brown, S., 1997. Use of humic acids to enhance the removal of aromatic hydrocarbons from contaminated aquifers. Report to GASReP, Groundwater Remediation Project, National Water Research Institute, Environment Canada.
Lewis, M.A., 1991. Chronic and sublethal toxicities of surfactants to aquatic animals, a review and risk assessment. Water Res. 25, 101–113.
Liu, H., Amy, G.L., 1993. Modelling partitioning and transport interactions between natural organic matter and polynuclear aromatic hydrocarbons on groundwater. Environ. Sci. Technol. 27 (8), 1553–1562.
Magee, B.R., Lion, L.W., Lemley, A.T., 1991. Transport of dissolved organic macromolecules and their effect on the transport of phenanthrene in porous media. Environ. Sci. Technol. 25 (2), 323–331.
Martel, R., Gelinas, P.K., Desnoyers, J., 1998. Aquifer washing by micellar solutions: 1. Optimization of alcohol–surfactant–solvent solutions. J. Contam. Hydrol. 29, 319–346.
Mayer, K.U., Frind, E.O., Blowes, D.W., 2001. Multicomponent reactive transport modeling in variably saturated porous media using generalized formulation for kinetically controlled reactions. J. Contam. Hydrol., submitted for publication.
McCarthy, J.F., Jiminez, B.D., 1985. Interactions between polycyclic aromatic hydrocarbons and dissolved humic material: binding and dissociation. Environ. Sci. Technol. 19, 1072–1076.
McCarthy, J.F., Zachara, J.M., 1989. Subsurface transport of contaminants. Environ. Sci. Technol. 23 (5), 496–502.
McCarthy, J.F., Gu, B., Liang, L., Mas-Pla, J., Williams, T.M., Yeh, T.-C.J., 1996. Field tracer tests on the mobility of natural organic matter in a sandy aquifer. Water Resour. Res. 32 (5), 1223–1238.
McCarthy, J.F., Czerwinsky, K.R., Sanford, W.E., Jardine, P.M., Marsh, J.D., 1998. Mobilization of transuranic radionuclides from disposal trenches by natural organic matter. J. Contam. Hydrol. 30, 49–77.
Molson, J.W., 2000a. BIONAPL/3D User Guide: A 3D Groundwater Flow, Multicomponent NAPL Dissolution and Reactive Transport Model.
Molson, J.W., 2000b. Numerical simulation of hydrocarbon fuel dissolution and biodegradation in groundwater. PhD Thesis, Dept. of Earth Sciences, University of Waterloo.

Neville, C.J., Ibaraki, M., Sudicky, E.A., 2000. Solute transport with multiprocess nonequilibrium: a semi-analytical approach. J. Contam. Hydrol. 44, 141–159.

Powers, S.E., Abriola, L.M., Dunkin, J.S., Weber, W.J., 1994. Phenomenological models for transient NAPL–water mass transfer processes. J. Contam. Hydrol. 16, 1–33.

Ramaswami, A., Luthy, R.G., 1997. Mass transfer and bioavailability of PAH compounds in coal tar NAPL–slurry systems: 1. Model development. Environ. Sci. Technol. 31, 2260–2267.

Rebhun, M., Smedt, F.D., Rwetabula, J., 1996. Dissolved humic substances for remediation of sites contaminated by organic pollutants: binding-desorption model predictions. Water Resour. Res. 30 (9), 2027–2038.

Rouse, J.D., Sabatani, D.A., Suflita, J.M., Harwell, J.H., 1994. Influence of surfactants on microbial degradation of organic compounds. Crit. Rev. Microb. Degrad. Org. Compd. 24, 325–370.

Schäfer, D., Schäfer, W., Kinzelbach, W., 1998. Simulation of reactive processes related to biodegradation in aquifers: 1. Structure of the three-dimensional reactive transport model. J. Contam. Hydrol. 31, 167–186.

Schirmer, M., Frind, E.O., Molson, J.W., 1995. Transport and biodegradation of hydrocarbons in shallow aquifers: 3D modeling. API Workshop: Comparative Evaluation of Groundwater Biodegradation Models, Fort Worth, Texas.

Schirmer, M., Molson, J.W., Frind, E.O., Barker, J.F., 2000. Biodegradation modelling of a dissolved gasoline plume applying independent laboratory and field parameters. J. Contam. Hydrol. 46, 339–374.

Tiehm, A., 1994. Degradation of polycyclic aromatic hydrocarbons in the presence of synthetic surfactants. Appl. Environ. Microbiol. 60, 258–263.

Totsche, K.U., Danzer, J., Koegel-Knabner, I., 1997. Dissolved organic matter-enhanced retention of polycyclic aromatic hydrocarbons in soil miscible displacement experiments. J. Environ. Qual. 26, 1090–1100.

Van Stempvoort, D., Lesage, R., 2001. Sorption of methylated naphthalenes by winter sand, a model aquifer material. Report for the Panel on Energy Research and Development (Part 4), NWRI Contribution No. 00-081, 20 pp.

Van Stempvoort, D.R., Lesage, S., 2002. Binding of methylated naphthalenes to concentrated aqueous humic acid. Adv. Environ. Res. (in press).

Van Stempvoort, D.R., Molson, J.W., Lesage, S., Brown, S., 2000. Sorption of aldrich humic acid to a test aquifer material and implications for subsurface remediation. In: Ghabbour, E.A., Davies, G. (Eds.), Humic Substances: Versatile Components of Plants, Soils and Water. Royal Society of Chemistry, Cambridge, UK, pp. 153–163.

Vermeer, A.W.P., van Riemsdijk, W.H., Koopal, L.K., 1998. Adsorption of humic acid to mineral particles: 1. Specific and electrostatic interactions. Langmuir 14, 2810–2819.

Warwick, P.W., Hall, A., Pashley, V., Bryan, N.D., Griffin, D., 2000. Modelling the effect of humic substances on the transport of europium through porous media. J. Contam. Hydrol. 42 (1), 19–34.

Widdowson, M.A., Molz, F.J., Benefield, L.D., 1988. A numerical transport model for oxygen and nitrate based respiration linked to substrate and nutrient availability in porous media. Water Resour. Res. 24, 1553–1565.

Wiedemeier, T.H., Rifai, H.S., Newell, C.J., Wilson, J.T., 1999. Natural Attenuation of Fuels and Chlorinated Solvents in the Subsurface. Wiley, New York.

Zhang, Y., Maier, W.J., Miller, R.M., 1997. Effect of rhamnolipids on the dissolution, bioavailability and biodegradation of phenanthrene. Environ. Sci. Technol. 31 (8), 2211–2217.

The scope of this journal will cover diverse topics including: experimental investigations of contaminant sorption, diffusion, transformations, volatilization and transport in the unsaturated and the saturated zones; characterization of soil and aquifer properties, but only as they influence contaminant behaviour; development and testing of mathematical models of contaminant behaviour; innovative techniques for restoration of contaminated sites; and development of new tools or techniques for monitoring the extent of soil and groundwater contamination.

Publication information
Journal of Contaminant Hydrology (ISSN 0169–7722). For 2002, volumes 53–59 are scheduled for publication. Subscription prices are available upon request from the Publisher or from the Regional Sales Office nearest you or from this journal's website (http://www.elsevier.com/locate/conhyd). Further information is available on this journal and other Elsevier Science products through Elsevier's website: (http://www.elsevier.com). Subscriptions are accepted on a prepaid basis only and are entered on a calendar year basis. Issues are sent by standard mail (surface within Europe, air delivery outside Europe). Priority rates are available upon request. Claims for missing issues should be made within six months of the date of dispatch.

New York, Elsevier Science, P.O. Box 945, New York, NY 10159-0945, USA. Tel: (+1) 212-633-3730, [Toll free number for North American Customers: 1-888-4ES-INFO (437-4636)], Fax: (+1) 212-633-3680, E-mail: usinfo-f@elsevier.com
Amsterdam, Elsevier Science, P.O. Box 211, 1000 AE Amsterdam, The Netherlands. Tel: (+31) 20-485-3757, Fax: (+31) 20-485-3432, E-mail: nlinfo-f@elsevier.nl
Tokyo, Elsevier Science K.K., 9-15, Higashi-Azabu 1-chome, Minato-ku, Tokyo 106-0044, Japan. Tel: (+81) 3-5561-5033, Fax: (+81) 3-5561-5047, Email: info@elsevier.co.jp
Singapore, Elsevier Science, No. 1 Temasek Avenue, #17-01 Millenia Tower, Singapore 039192. Tel: (+65) 434-3727, Fax: (+65) 337-2230, E-mail: asiainfo@elsevier.com.sg
Rio de Janeiro, Elsevier Science, Rua Sete de Setembro 111/16 Andar, 20050-002 Centro, Rio de Janeiro - RJ, Brazil; phone: (+55) (21) 509 5340; fax: (+55) (21) 507 1991; e-mail: elsevier@campus.com.br [Note (Latin America): for orders, claims and help desk information, please contact the Regional Sales Office in New York as listed above]

USA mailing notice: *Journal of Contaminant Hydrology* (ISSN 0169-7722) is published monthly by Elsevier Science B.V. (P.O. Box 211, 1000 AE Amsterdam, The Netherlands). Annual subscription price in the USA US$ 1863 (valid in North, Central and South America), including air speed delivery. Application to mail at periodical postage rate is pending at Jamaica, NY 11431.
USA POSTMASTER: Send address changes to *Journal of Contaminant Hydrology,* Publications Expediting Inc., 200 Meacham Ave, Elmont, NY 11003.
AIRFREIGHT AND MAILING in the USA by Publications Expediting Inc., 200 Meacham Avenue, Elmont, NY 11003.

Environment Canada Environnement Canada

Canada

Canada Centre for Inland Waters
P.O. Box 5050
867 Lakeshore Road
Burlington, Ontario
L7R 4A6 Canada

National Hydrology Research Centre
11 Innovation Boulevard
Saskatoon, Saskatchewan
S7N 3H5 Canada

St. Lawrence Centre
105 McGill Street
Montreal, Quebec
H2Y 2E7 Canada

Place Vincent Massey
351 St. Joseph Boulevard
Gatineau, Quebec
K1A 0H3 Canada

Centre canadien des eaux intérieures
Case postale 5050
867, chemin Lakeshore
Burlington (Ontario)
L7R 4A6 Canada

Centre national de recherche en hydrologie
11, boul. Innovation
Saskatoon (Saskatchewan)
S7N 3H5 Canada

Centre Saint-Laurent
105, rue McGill
Montréal (Québec)
H2Y 2E7 Canada

Place Vincent-Massey
351 boul. St-Joseph
Gatineau (Québec)
K1A 0H3 Canada